

Criticality and isostaticity in fiber networks

Chase P. Broedersz,¹ Xiaoming Mao,² T.C. Lubensky,² and F.C. MacKintosh¹

¹*Department of Physics and Astronomy, Vrije Universiteit, Amsterdam, The Netherlands*

²*Department of Physics and Astronomy, University of Pennsylvania, Philadelphia, Pennsylvania 19104, USA*

(Dated: August 15, 2018)

The rigidity of elastic networks depends sensitively on their internal connectivity and the nature of the interactions between constituents. Particles interacting via central forces undergo a zero-temperature rigidity-percolation transition near the isostatic threshold, where the constraints and internal degrees of freedom are equal in number^{1,2}. Fibrous networks, such as those that form the cellular cytoskeleton^{3,4}, become rigid at a lower threshold due to additional bending constraints. However, the degree to which bending governs network mechanics remains a subject of considerable debate^{5–12}. We study disordered fibrous networks with variable coordination number, both above and below the central-force isostatic point. This point controls a broad crossover from stretching- to bending-dominated elasticity. Strikingly, this crossover exhibits an anomalous power-law dependence of the shear modulus on *both* stretching and bending rigidities. At the central-force isostatic point—well above the rigidity threshold—we find divergent strain fluctuations together with a divergent correlation length ξ , implying a breakdown of continuum elasticity in this simple mechanical system on length scales less than ξ .

There are numerous examples of stiff-fiber networks, ranging from carbon nanotube gels at the small scale to felt and paper at the macroscopic scale^{13–15}. In addition, critical biological components such as the intra-cellular cytoskeleton and extra-cellular matrices of collagen and fibrin are composed of such networks¹⁶. Here, we use a combination of simulations and effective medium theory we study the elasticity of disordered fiber networks composed of straight, stiff filaments organized on a triangular lattice in 2D and face centered cubic (FCC) lattice in 3D, as illustrated in Fig. 1. Undiluted, these networks have a coordination number $z_m = 6$ (triangular lattice) and $z_m = 12$ (FCC), placing them well above the central-force (CF) isostatic point $z_c = 2d$ in d dimensions^{1,17}. We explore the effects of network connectivity—both above and below z_c —by removing filament segments between vertices with a probability $1 - p$.

The mechanical response of the fibers in the network is determined by their bending rigidity κ and stretching modulus μ . For small deformations, the stretching and bending energy of the network can be expanded to quadratic order in the displacements \mathbf{u}_i from the unde-

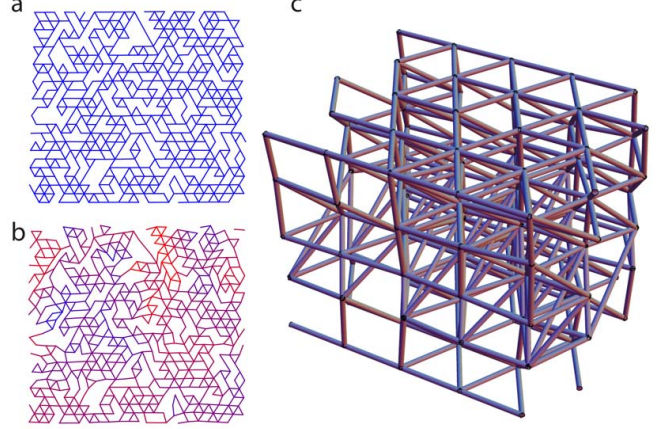


FIG. 1: **Fiber networks arranged on 2D and 3D lattices** A small section of a sheared diluted triangular network near isostaticity with relatively stiff filaments ($\kappa = 10^1$ in units of $\mu\ell_0^2$) (a) and floppy filaments ($\kappa = 10^{-5}$) (b). The deviation of the local deformation from a uniform or affine deformation is indicated by color, where blue corresponds to a uniform or affine deformation and red corresponds to a highly non-affine deformation. (c) An example of a small section of the diluted FCC network at $p = 0.7$. To probe the mechanical properties of this network we shear the 111-plane (shown on top) along the direction of one of the bond angles in this plane.

formed reference state at each vertex i ,

$$E_{\text{stretch}} = \frac{1}{2} \frac{\mu}{\ell_0} \sum_{\langle ij \rangle} g_{ij} (\mathbf{u}_{ij} \cdot \hat{\mathbf{r}}_{ij})^2 \quad (1)$$

$$E_{\text{bend}} = \frac{1}{2} \frac{\kappa}{\ell_0^3} \sum_{\langle ijk \rangle} g_{ij} g_{jk} [(\mathbf{u}_{jk} - \mathbf{u}_{ij}) \times \hat{\mathbf{r}}_{ij}]^2, \quad (2)$$

where ℓ_0 is the lattice spacing, $\mathbf{u}_{ij} = \mathbf{u}_j - \mathbf{u}_i$ and $\hat{\mathbf{r}}_{ij}$ is the unit vector oriented along the ij -th bond in the undeformed reference state. Here, $g_{ij} = 1$ for present bonds and $g_{ij} = 0$ for removed bonds. The summation extends over neighboring pairs of vertices in the stretching term [Eq. (1)], and over coaxial neighboring bonds in the bending term [Eq. (2)]. Thus, in our networks the cross-links at each vertex are freely hinging.

To investigate the mechanical response of a network, we calculate its shear modulus G numerically. The diluted networks exhibit a finite shear modulus well below the CF isostatic point (expected at $p_c = 2/3$ in 2D and $p_c = 1/2$ in 3D), as shown in Fig. 2a,b; G vanishes at a κ -independent rigidity percolation point located at $p_b = 0.445 \pm 0.005$ (2D triangular lattice) and $p_b = 0.275 \pm 0.005$ (3D FCC lattice), consistent with a

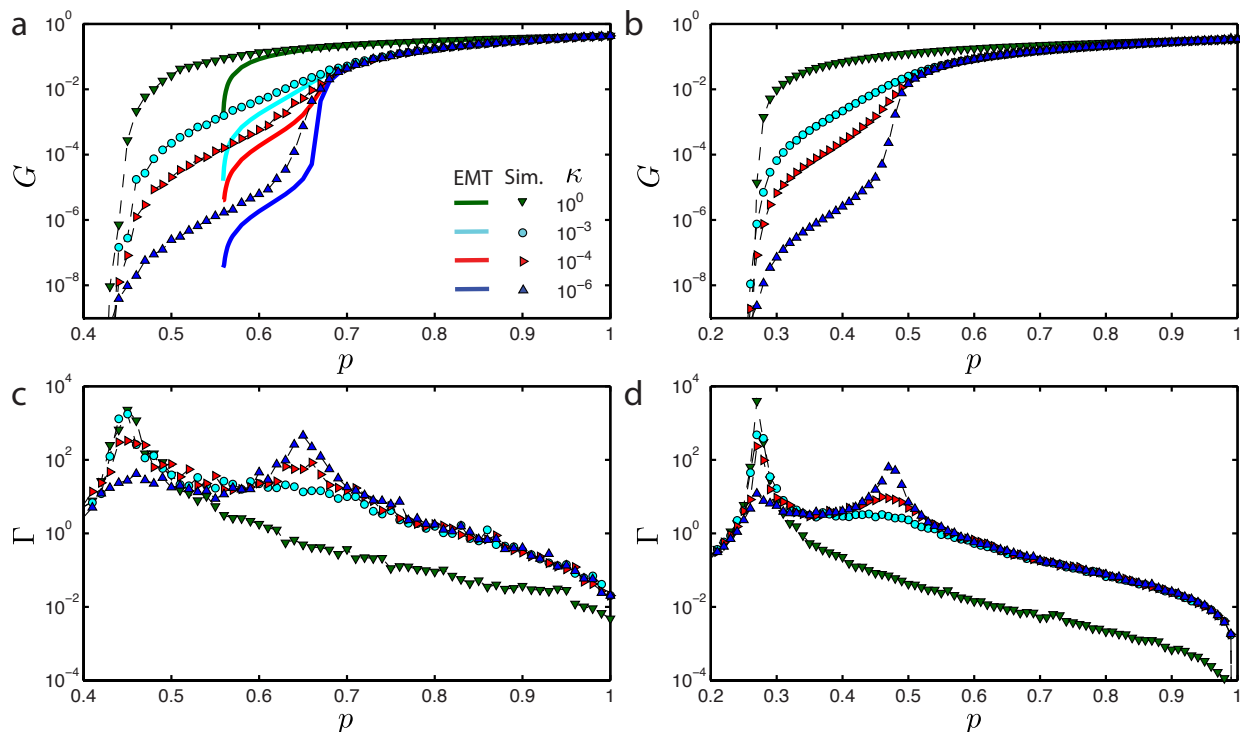


FIG. 2: **Mechanics and non-affine strain fluctuations** The shear modulus G in units of μ/ℓ_0 as a function of p for a range of filament bending rigidities κ for the 2D triangular lattice (a) and the 3D FCC lattice (b). The EMT calculations for the 2D triangular lattice are shown as solid lines. The non-affinity measure Γ is shown as a function of p for various values of κ for the 2D triangular lattice (c) and the 3D FCC lattice (d). The values of κ in units of $\mu\ell_0^2$ are 10^0 (green), 10^{-3} (cyan), 10^{-4} (red) and 10^{-6} (blue).

floppy mode counting argument that includes the bending constraints (suppl. info.). Plots of G versus p for different κ are shown for the triangular and FCC lattices in Figs. 2 a,b. For $p > p_c$, G approaches a nearly κ -independent stretching dominated limit with $G \sim \mu$. In contrast, for $p < p_c$, G falls off reaching a bending dominated limit with $G \sim \kappa$ as $p \rightarrow p_b$. The most interesting behavior occurs near p_c as a function of κ . There is a stretch dominated regime at large κ and bending dominated one at small κ with a broad intermediate crossover regime with G depending on both κ and μ .

To gain insight into the mechanical behavior of our models, we developed a new effective medium theory (EMT) or coherent potential approximation (CPA)^{18–20} for lattices with bending forces, which we discuss in more detail in the methods section, whose results for G for different κ are shown in Fig. 2a. These results overestimate the rigidity percolation point p_b . Nonetheless, this model captures the essential features of the simulations well, including the crossover between stretching and bending dominated regimes close to p_c . Our EMT theory predicts that when $\kappa/\mu \ll \Delta p$, G can be expressed in the vicinity of p_c in the scaling form

$$G = \mu |\Delta p|^f \mathcal{G}_{\pm} \left(\frac{\kappa}{\mu} |\Delta p|^{-\phi} \right), \quad (3)$$

where $f = f_{\text{EMT}} = 1$ and $\phi = \phi_{\text{EMT}} = 2$ are, respectively,

the rigidity and crossover critical exponents. This scaling form is analogous to that for the conductivity of a random resistor network²¹ with bonds occupied with resistors of conductance $\sigma_>$ and $\sigma_<$ with respective probabilities p and $(1-p)$. When $y \ll 1$, $\mathcal{G}_+(y) \sim \text{const.}$ and $\mathcal{G}_-(y) \sim y$ implying $G \sim \mu |\Delta p|^f$ for $\Delta p > 0$ and $G \sim \kappa |\Delta p|^{f-\phi}$ for $\Delta p < 0$. In the opposite limit $(\kappa/\mu) \gg |\Delta p|^\phi$, G must become independent of Δp since it is neither zero nor infinite at $\Delta p = 0$. Equation (3) predicts $G \sim \kappa^{f/\phi} \mu^{1-(f/\phi)}$, which reduces to $G \sim \kappa^{1/2} \mu^{1/2}$ in the EMT theory. The full EMT results for G along with the scaling form valid at $\kappa/\mu \ll |\Delta p|^\phi$ are shown in Fig. 3a.

Our simulation data for both 2D and 3D networks are well described by the scaling hypothesis in Eq. (3), consistent with a second-order transition for $\kappa = 0$ in both cases²². Fig. 3b shows the results for both the triangular case and FCC cases (inset). As expected from previous simulation work^{5,6,12}, we find a bending-dominated regime at small κ and a stretching-dominated regime at large κ . Consistent with the EMT prediction above, we find a previously unexpected intermediate regime with $G \sim \kappa^x \mu^{1-x}$ where $x = f/\phi \approx 0.50 \pm 0.01$ (2D) and $f/\phi \approx 0.40 \pm 0.01$ (3D). These results are consistent with our exponents obtained above (Table 1, suppl. info.). While the extent of this intermediate regime is bounded from above by the affine modulus, it can extend to arbitrarily small $\kappa > 0$ as the system is brought closer to CF

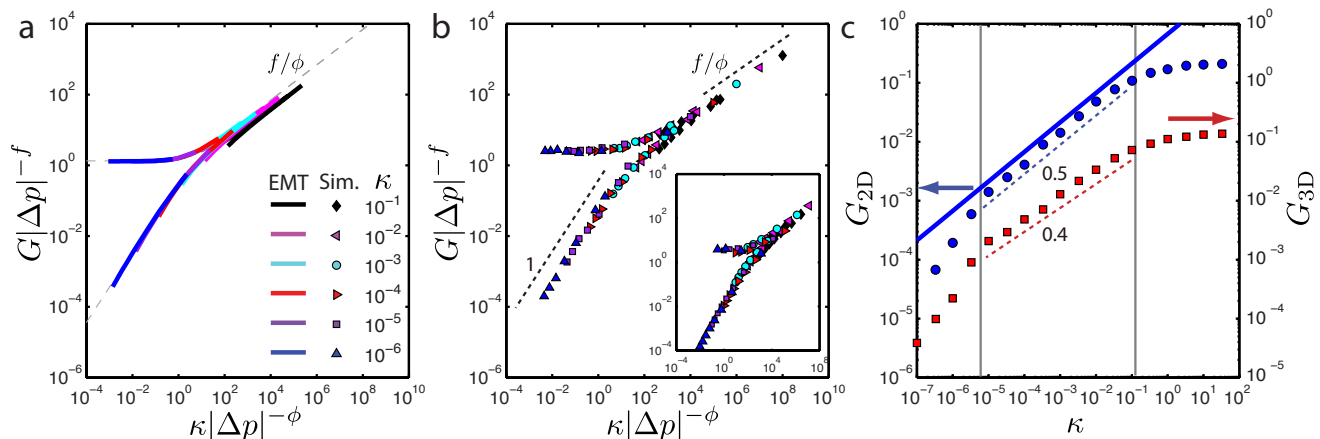


FIG. 3: **Scaling analysis of the mechanics and anomalous elasticity** Scaling of the shear modulus in the vicinity of the isostatic point with the scaling form $G|\Delta p|^{-f} = \mathcal{G}_{\pm}(\kappa|\Delta p|^{-\phi})$, with G in units of μ/ℓ_0 , for the mechanical properties of the diluted triangular lattice for the EMT calculations (a) and the simulations (b) for a broad range of filament bending rigidities (κ in units of $\mu\ell_0^2$: 10^{-1} black, 10^{-2} magenta, 10^{-3} cyan, 10^{-4} red, 10^{-5} purple and 10^{-6} blue). The asymptotic form of the scaling function for low κ is shown as a dashed grey line in (a). The scaling for the numerical data on the 3D FCC lattice is shown as an inset in b. The EMT exponents are $f_{\text{EMT}} = 1$, $\phi_{\text{EMT}} = 2$. In contrast, for the numerical data we obtain $f = 1.4 \pm 0.1$, $\phi = 3.0 \pm 0.2$ (2D) and $f = 1.6 \pm 0.2$, $\phi = 3.6 \pm 0.3$ (3D). The scaling for the numerical data is performed with respect to the isostatic point of the finite system for which we find $p_c(W) \approx 0.651$ (2D, $W=200$) and $p_c(W) \approx 0.473$ (3D, $W=30$). (c) The shear modulus as a function of κ close to the isostatic point for the triangular lattice ($p = 0.643$, blue circles) and the FCC lattice ($p = 0.47$, red squares). At low κ there is a bending dominated regime $G_{\text{bend}} \sim \kappa$, at intermediate κ there is a regime in which stretching and bending modes couple strongly with $G \sim \mu^{1-x}\kappa^x$, where $x = 0.50 \pm 0.01$ (2D) and $x \approx 0.40 \pm 0.01$ (3D). The EMT calculation for $\kappa/\mu \gg |\Delta p|^{\phi_{\text{EMT}}}$ is shown as a solid blue line.

isostaticity.

To investigate the nature of the various mechanical regimes, we examine the local deformation field in our simulations. Several methods have been proposed to quantify the deviation from a uniform (affine) strain field^{5,23,24}. Here we utilize a measure for this non-affinity given by

$$\Gamma = \frac{1}{N\gamma^2} \sum_i [\mathbf{u}_i - \mathbf{u}_i^{(\text{aff})}]^2, \quad (4)$$

where $\mathbf{u}_i^{(\text{aff})}$ is the affine displacement of vertex i and N is the number of vertices. This quantity varies over eight orders of magnitude, indicating non-affine fluctuations that depend strongly on both κ and p , as shown in Figs. 2c,d. For stretch-dominated networks (high κ), we find a monotonic increase in non-affine fluctuations with decreasing p , which appear to diverge at p_b . Remarkably, for smaller values of κ , a second peak in Γ develops at p_c . Importantly, the development of this peak coincides with the appearance of a crossover between the stretching and bending regimes (Figs. 2a-d).

The critical behavior we observe suggests both a divergence of the non-affine fluctuations according to¹⁷ $\Gamma = \Gamma_{\pm}|\Delta p|^{-\lambda}$ and the existence of a divergent length-scale $\xi = \xi_{\pm}|\Delta p|^{-\nu}$ near the critical point P_c for vanishing κ . However, the divergence of ξ is limited by the system size W , which should suppress the divergence of Γ . Consistent with this picture, we find that the location of the cusp in the local fluctuations

Γ shift towards higher p with increasing W according to $p_c(W) = p_c + bW^{-1/\nu}$, with $\nu = 1.4 \pm 0.2$ and $p_c = 0.659 \pm 0.002$ (suppl. info.); these values are consistent with previous reports on generic CF networks²⁵. In addition, the amplitude of Γ increases with system size (Fig. 4a), in quantitative accord with the expected finite-size scaling. Specifically, we find a good collapse of the simulation data with $\Gamma = W^{\lambda/\nu} \mathcal{F}_{\Gamma,\pm}(|\Delta p|W^{1/\nu})$ over a range of system sizes, with $\lambda/\nu = 1.6 \pm 0.2$ and $\nu = 1.4 \pm 0.2$, as shown in Fig. 4b. Similarly, the shear modulus exhibits finite-size scaling (Suppl. info.) according to $G = W^{-f/\nu} \mathcal{F}_{G,\pm}(|\Delta p|W^{1/\nu})$, as shown in Fig. 4c. We obtain a good collapse of the elasticity data using $f/\nu = 0.9 \pm 0.1$, along with ν determined from the finite-size scaling of Γ (Fig. 4b and suppl. info), consistent with the value of f obtained from the scaling in Fig. 3. Thus, we find a scale-dependence of the shear modulus that is consistent with critical behavior governed by the CF isostatic critical point. Furthermore, the critical behavior in these purely mechanical networks is accompanied by shear-induced divergent non-affine fluctuations. These results imply a breakdown of continuum elasticity below the divergent length-scale ξ .

The undiluted triangular and FCC lattices we study have an average coordination number greater than $2d$ and thus are above the Maxwell central-force isostatic threshold. These networks also consist of infinitely long filaments. Cutting bonds as we do introduces both finite length polymers, as well as lower connectivity, down to the CF threshold and below. Cytoskeletal and extracel-

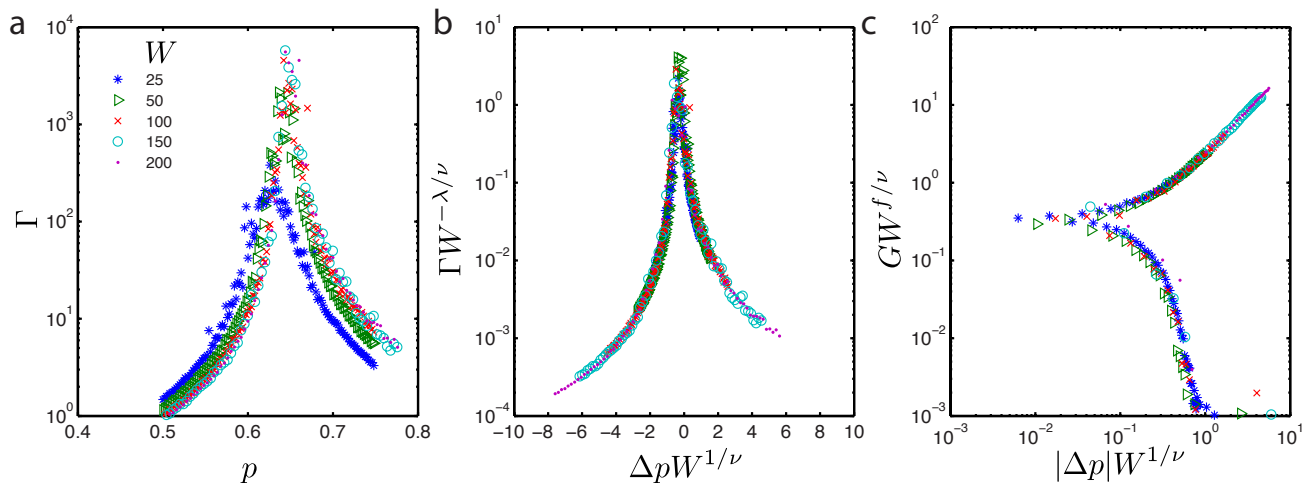


FIG. 4: **Finite size scaling** (a) The non-affinity measure Γ for the 2D triangular lattice at $\kappa = 0$ for various systems sizes W (25 blue, 50 green, 100 red, 150 cyan and 200 purple). Finite size scaling of the non-affinity measure Γ according to the scaling form $\Gamma = W^{\lambda/\nu} \mathcal{F}_{\Gamma, \pm}(\Delta p W^{1/\nu})$ (b) and of the shear modulus with the scaling form $G = W^{-f/\nu} \mathcal{F}_{G, \pm}(|\Delta p| W^{1/\nu})$ (c). Here $\Delta p = p - p_c$, where $p_c = 0.659 \pm 0.002$. The exponents we obtain are $\lambda/\nu = 1.6 \pm 0.2$, $\nu = 1.4 \pm 0.2$ and $f/\nu = 0.9 \pm 0.1$.

lular networks can have z as low as 3 (e.g., in branched networks) and as high as 6 (in the case of actin-spectrin networks), although they typically have a local connectivity $z \simeq 4$, where two filaments are connected by a crosslink. As a consequence, the CF isostatic point is expected to occur for high molecular weight in 2D. We conjecture that there is an analogous crossover behavior for such networks, including the anomalous scaling behavior for the elasticity. In addition, we expect that our results for the crossover behavior will apply to bond-bending models on similar lattices to ours^{2,26–28} for rigidity percolation and network glasses that include bending forces between bonds pairs at each network node. Finally, from the perspective of critical phenomena more generally, the kind of crossover behavior we find here is in contrast to most thermal systems, where a field or coupling constant leads to a crossover from one critical system to another, such as from the Heisenberg model to the Ising model³⁰. In such systems, there is a continuous evolution of the critical point that is governed by the crossover exponent ϕ . Interestingly, we find no such continuous evolution, but rather a discontinuous jump in the critical point p_c as soon as κ becomes nonzero.

I. METHODS

Simulations The mechanical response of the network is determined in our simulations by applying a shear deformation with a strain γ . This is realized by translating the horizontal boundaries to which the filaments are attached, after which the internal degrees of freedom are relaxed by minimizing the energy using a conjugate gradient algorithm²⁹. To reduce edge effects in our simulation, periodic boundary conditions are employed at all boundaries. The shear modulus of the network is re-

lated to the elastic energy through $G = \frac{2}{V_0 W^d} \frac{E}{\gamma^2}$ for a small strain γ , where V_0 is the area/volume of a unitcell. Here W^d is the system size, which in our simulations is $W^2 \approx 40000$ (2D) and $W^3 \approx 30000$ (3D), and we used strains no larger than $\gamma = 0.05$.

EMT The EMT maps the diluted random network to an undiluted uniform effective medium (EM) with respective stretching modulus μ_m and bending rigidity κ_m , which are determined self-consistently as follows. In our theory, κ is as a property of the filament connecting neighboring sites rather than as a site-associated rigidity that connects next-nearest neighbor sites. Following standard EM procedures, an arbitrary bond is either replaced with probability p by a bond of stretching modulus μ and bending rigidity κ or removed with probability $1 - p$. The phonon Green's function after this replacement is calculated as a perturbation with respect to the uniform effective medium, treating the replaced bond as a scattering potential V on the EM Hamiltonian. The EMT self-consistency condition requires that the disorder-averaged Green's function equals that of the unperturbed EM, i.e., that the average \mathbf{T} -matrix arising from the perturbed bond vanishes, giving us equations determining μ_m and κ_m for given p .

In the EMT scattering potential V , the stretching term is simply proportional to $\mu - \mu_m$ if the bond is occupied and $-\mu_m$ if it is removed. The bending terms must, however, be treated differently because replacing a bond generates two bending terms, both of which involve second-neighbor interactions. This can be understood by considering 4 sites $ijkl$ along a filament. If one replaces bond jk , two bending terms involving second-neighbors ijk and jkl are generated in V . The coefficients of these two bending terms can be found by considering a composite filament connecting $ijkl$ that is composed of rods with bending rigidity κ_s between sites jk and κ_m between

sites ij and jk , respectively, where $\kappa_s = \kappa$ if the bond is occupied and $\kappa_s = 0$ if it is removed. A direct calculation of the minimum bending energy yields the effective bending rigidity

$$\kappa_c = 2\left(\frac{1}{\kappa_s} + \frac{1}{\kappa_m}\right)^{-1}, \quad (5)$$

and thus the coefficients of the two bending terms involving ijk and jkl in V is given by $\kappa_c - \kappa_m$.

To close the EMT self-consistency equation,

$$p\mathbf{T}(\mu, \kappa) + (1-p)\mathbf{T}(0, 0) = 0, \quad (6)$$

where \mathbf{T} is the \mathbf{T} -matrix constructed from the perturbation of the scattering potential V , a third-neighbor coupling λ_m

$$\frac{1}{2}\lambda_m \sum_{\langle ijkl \rangle} [(\mathbf{u}_{jk} - \mathbf{u}_{ij}) \times \hat{\mathbf{r}}_{ij}] [(\mathbf{u}_{kl} - \mathbf{u}_{jk}) \times \hat{\mathbf{r}}_{kl}] \quad (7)$$

must be introduced to the EM and to V accordingly. Thus the EM is characterized by 3 parameters $(\mu_m, \kappa_m, \lambda_m)$, determined by the self-consistency equation (6). We obtained asymptotic solutions to this equation for small κ in the vicinity of the CF isostatic point, in which μ_m can be written into a scaling form same as that of Eq. (3) by identifying that the shear modulus $G = \sqrt{3}\mu_m/4$, and the scaling function is

$$\mathcal{G}_{\pm}(y) \simeq \frac{3}{2}(\pm 1 + \sqrt{1 + 4\mathcal{A}y/9}) \quad (8)$$

with $\mathcal{A} \simeq 2.413$.

For $\kappa/\mu \ll |\Delta p|^{\phi_{\text{EMT}}}$, to leading order, the value for μ_m reduces to $3\mu|\Delta p|$ for $\Delta p > 0$, and $\frac{4}{3}\kappa|\Delta p|^{-1}$ for $\Delta p < 0$. For $\kappa/\mu \gg |\Delta p|^{\phi_{\text{EMT}}}$ we get $\mu_m \simeq \sqrt{\mathcal{A}}\mu^{1/2}\kappa^{1/2}$. These three scaling regimes correspond to three different slopes 0, 1, 1/2 in the $G|\Delta p|^{-f}$ vs $\kappa|\Delta p|^{-\phi}$ plot, as shown in Fig. 3a.

Effective medium theories for bond-diluted lattices with central-force springs are straightforward because the springs reside on an individual bond. In contrast, EMTs for lattices with bending forces are less so because bending forces reside on two bonds and dilution removes only a single bond at a time. Our solution is to treat a given bond as a filament segment with bending modulus κ_s . The effective lattice bending modulus for neighboring

bonds with respective bending moduli κ_b and κ_m is given by Eq. (5). This treatment allows us to unambiguously remove one bond at a time. The resultant effective theory necessarily includes bend-stretch coupling. A previous EMT theory²⁰ treated the bending problem by removing two bonds at a time. The result was a theory that lacks bend-stretch coupling and predicted separate thresholds for the development of non-vanishing μ_m and κ_m , which is inconsistent with both the numerical and analytical EMT results presented here.

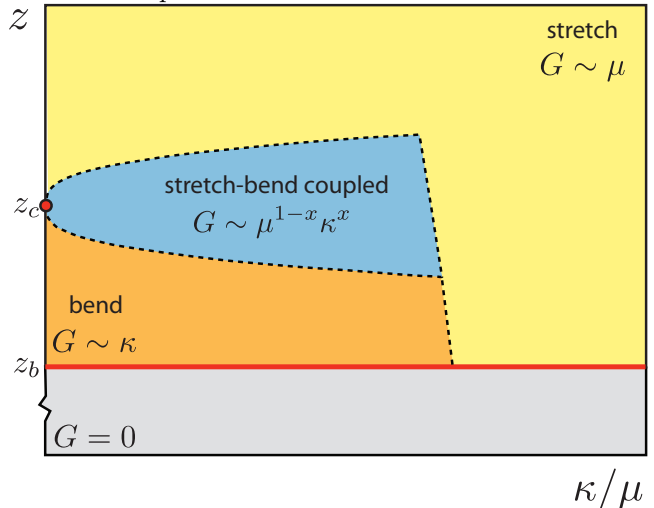


FIG. 5: **Phase diagram** The phase diagram for diluted super-isostatic networks. Above the rigidity percolation point z_b there are three distinct mechanical regimes: a stretching dominated regime with $G \sim \mu$, a bending dominated regime with $G \sim \kappa$ and a regime in which bend and stretch modes couple with $G \sim \mu^{1-x}\kappa^x$. Here x is related to the critical exponents $x = f/\phi$. We find here that $x = 0.50 \pm 0.01$ (2D triangular lattice) and $x = 0.40 \pm 0.01$ (3D FCC). The mechanical regimes are controlled by the isostatic point z_c , which acts as a zero-temperature critical point.

Acknowledgments

This work was supported in part by NSF-DMR-0804900 (TCL and XM) and in part by FOM/NWO (CPB and FCM). The authors thank M. Das and L. Jawerth for useful discussions.

CPB and FCM designed the simulation model, which was developed and executed by CPB. XM and TCL developed and executed the EMT. All authors contributed to the writing of the paper.

¹ Maxwell, J. C. On the calculation of the equilibrium and stiffness of frames. *Philos. Mag.* **27**, 294 (1864).

² Thorpe, M. Continuous deformations in random networks. *J. Non-Cryst. Solids* **57**, 355 – 370 (1983).

³ Bausch, A. & Kroy, K. A bottom-up approach to cell mechanics. *Nature Phys.* **2**, 231–238 (2006).

⁴ Fletcher, D. & Mullins, R. Cell mechanics and the cytoskeleton. *Nature* **463**, 485–492 (2010).

⁵ Head, D. A., Levine, A. J. & MacKintosh, F. C. Deformation of cross-linked semiflexible polymer networks. *Phys. Rev. Lett.* **91**, 108102 (2003).

⁶ Wilhelm, J. & Frey, E. Elasticity of stiff polymer networks.

- Phys. Rev. Lett.* **91**, 108103 (2003).
- ⁷ Gardel, M. L. *et al.* Elastic Behavior of Cross-Linked and Bundled Actin Networks. *Science* **304**, 1301–1305 (2004).
 - ⁸ Storm, C., Pastore, J., MacKintosh, F., Lubensky, T. & Janmey, P. Nonlinear elasticity in biological gels. *Nature* **435**, 191–194 (2005).
 - ⁹ Onck, P. R., Koeman, T., van Dillen, T. & van der Giessen, E. Alternative explanation of stiffening in cross-linked semiflexible networks. *Phys. Rev. Lett.* **95**, 178102 (2005).
 - ¹⁰ Heussinger, C. & Frey, E. Floppy modes and nonaffine deformations in random fiber networks. *Phys. Rev. Lett.* **97**, 105501 (2006).
 - ¹¹ Chaudhuri, O., Parekh, S. & Fletcher, D. Reversible stress softening of actin networks. *Nature* **445**, 295–298 (2007).
 - ¹² Buxton, G. A. & Clarke, N. “Bending to stretching” transition in disordered networks. *Phys. Rev. Lett.* **98**, 238103 (2007).
 - ¹³ Hall, L. J. *et al.* Sign Change of Poisson’s Ratio for Carbon Nanotube Sheets. *Science* **320**, 504–507 (2008).
 - ¹⁴ Hough, L. A., Islam, M. F., Janmey, P. A. & Yodh, A. G. Viscoelasticity of single wall carbon nanotube suspensions. *Phys. Rev. Lett.* **93**, 168102 (2004).
 - ¹⁵ Kabla, A. & Mahadevan, L. Nonlinear mechanics of soft fibrous networks. *J. R. Soc. Interface* **4**, 99–106 (2007).
 - ¹⁶ Pedersen, J. & Swartz, M. Mechanobiology in the third dimension. *Ann. Biomed. Eng.* **33**, 1469–1490 (2005).
 - ¹⁷ Wyart, M., Liang, H., Kabla, A. & Mahadevan, L. Elasticity of floppy and stiff random networks. *Phys. Rev. Lett.* **101**, 215501 (2008).
 - ¹⁸ Soven, P. Contribution to the theory of disordered alloys. *Phys. Rev.* **178**, 1136–1144 (1969).
 - ¹⁹ Feng, S., Thorpe, M. F. & Garboczi, E. Effective-medium theory of percolation on central-force elastic networks. *Phys. Rev. B* **31**, 276–280 (1985).
 - ²⁰ Das, M., MacKintosh, F. C. & Levine, A. J. Effective medium theory of semiflexible filamentous networks. *Phys. Rev. Lett.* **99**, 038101 (2007).
 - ²¹ Straley, J. Critical phenomena in resistor networks. *J. Phys. C: Solid State Phys.* **9**, 783 (1976).
 - ²² Chubynsky, M. V. and Thorpe, M. F. Algorithms for three-dimensional rigidity analysis and a first-order percolation transition. *Phys. Rev. E* **76**, 041135 (2007).
 - ²³ DiDonna, B. A. & Lubensky, T. C. Nonaffine correlations in random elastic media. *Phys. Rev. E* **72**, 066619 (2005).
 - ²⁴ Liu, J., Koenderink, G. H., Kasza, K. E., MacKintosh, F. C. & Weitz, D. A. Visualizing the strain field in semiflexible polymer networks: Strain fluctuations and nonlinear rheology of *f*-actin gels. *Phys. Rev. Lett.* **98**, 198304 (2007).
 - ²⁵ Jacobs, D. J. & Thorpe, M. F. Generic rigidity percolation in two dimensions. *Phys. Rev. E* **53**, 3682–3693 (1996).
 - ²⁶ Schwartz, L. M., Feng, S., Thorpe, M. F. & Sen, P. N. Behavior of depleted elastic networks - comparison of effective-medium and numerical-calculations. *Phys. Rev. B* **32**, 4607–4617 (1985).
 - ²⁷ He, H. & Thorpe, M. F. Elastic properties of glasses. *Phys. Rev. Lett.* **54**, 2107–2110 (1985).
 - ²⁸ Sahimi, M. & Arbabi, S. Mechanics of disordered solids. ii. percolation on elastic networks with bond-bending forces. *Phys. Rev. B* **47**, 703–712 (1993).
 - ²⁹ Vetterling, W. T. & Flannery, B. P. *Numerical Recipes in C++: The Art of Scientific Computing, 2nd ed.* (Cambridge University Press, 2002).
 - ³⁰ Fisher, M. E., in *Proceedings of the School on Critical Phenomena, Stellenbosch, South Africa, 1982*, edited by F.J.W. Hahne (Springer-Verlag, Berlin, 1983), Vol. 186.